Evaluating edge loss in the reflectance measurement of translucent materials

Lou Gevaux, Lionel Simonot, Raphael Clerc, Morgane Gerardin, Mathieu Hebert

Evaluating edge-loss in the reflectance measurement of translucent materials

LOU GEVAUX,[1] LIONEL SIMONOT,[2,*] RAPHAEL CLERC,[1] MORGANE GERARDIN,[3,4] AND MATHIEU HEBERT[1]

[1]*Univ Lyon, UJM-Saint-Etienne, CNRS, Institut d Optique Graduate School, Laboratoire Hubert Curien UMR 5516, F-42023, Saint-Etienne, France*
[2]*Université de Poitiers, Institut Pprime UPR CNRS 3346, Futuroscope Chasseneuil, France*
[3]*Univ. Grenoble-Alpes, Inria, CNRS, Grenoble INP, LJK, F-38042, Grenoble, France*
[4]*Univ. Grenoble-Alpes, Inst NEEL, CNRS, F-38042, Grenoble, France*
**Corresponding author: lionel.simonot@univ-poitiers.fr*

Received XX Month XXXX; revised XX Month, XXXX; accepted XX Month XXXX; posted XX Month XXXX (Doc. ID XXXXX); published XX Month XXXX

Abstract: In many commercial instruments for measuring reflectance, the area illuminated on the measured object is identical to the area from which light is collected. This configuration is suitable for strongly scattering materials such as paper, but issues arise with translucent materials, as a portion of the incident light spreads around the illuminated area by subsurface transport and escapes the detection system. This phenomenon, referred to as edge-loss, yields erroneous, underestimated reflectance measurements. In the case of colored and opalescent materials, the impact of edge-loss on the measured reflectance varies with wavelength, which is a significant issue for spectrophotometer and colorimeter users. In the present study, we investigate the edge-loss phenomenon with an emphasis on human skin measurement. In particular, we use a mathematical model to estimate the PSF of translucent materials, relying on the diffusion approximation of the radiative transfer theory, to predict edge-loss measurement error. We use this model to discuss the suitability of several commercial spectrophotometers for accurately measuring translucent materials of various optical properties and show that not all devices are adapted to all translucent materials.

http://dx.doi.org/xxxx/AO.99.099999

1. INTRODUCTION

Spectral reflectance measurement is commonly used to characterize the visual appearance of objects or to study their optical properties. Since the way light is reflected by an object strongly depends on the object's material and surface properties, the reflectance measurement method must be adapted to each case. It is well known that a strongly specular object, such as a polished piece of metal, cannot be measured in the same way as a Lambertian object, such as a piece of rough paper [1]. In this study, we aim to provide more information on the measurement of samples made of translucent material. Translucent materials include marble, jade, resin-based composites, plastic, leaves, organic materials, biological tissues and human skin, and their measurement impacts applications in many domains including medicine, dermatology, dentistry, agronomy, 3D printing, cultural heritage and computer graphics.

A translucent material, also called a turbid material, can be defined as a scattering and absorbent material into which light can enter and propagate, before either being absorbed or re-exiting. For most exiting photons, the exit point differs from the entry point due to subsurface scattering. The probability for a photon to re-exit the material at a given location in function of its entry point is described by the material's *Point Spread Function* (PSF). This definition of translucency, which can be more precisely referred to as *optical translucency*, is an intrinsic property of the material revealed when illuminated on a finite area, and relates to its propensity to spread light due to subsurface scattering around the illuminated area. Optical translucency should not be mistaken for the visual sensation of translucency [2,3] that describes an object's appearance and depends on a multitude of parameters including the object's shape, surface properties, material properties, the lighting conditions, the observation being static or dynamic, as well as the interpretation of the light signal by the observer's brain. The perceptual translucency of an object is not always correlated to the optical translucency of the material that it is made of: under homogeneous illumination, a plate made of translucent material is perceived as translucent when it is thin enough to transmit light, and is perceived as opaque when it is sufficiently thick to prevent any light transmission. In this study, when we refer to translucent materials, we are referring to optical translucency, regardless of the visual appearance of the measured object itself. We also prefer the term "strongly scattering" to the term "opaque" to designate materials for which subsurface light transport is strongly limited, i.e. materials

for which any incident ray is absorbed or backscattered so quickly that the distance it can travel within the material is almost zero.

When a translucent material is illuminated on a finite area, part of the reflected light exits the material outside the illuminated area, creating a blurring effect at the edges. When measuring reflectance, this lateral spread of light can yield incorrect measurements: if the area observed by the light collection system coincides with the illuminated area, the light exiting the material outside the illuminated area is out of the scope of the light collection system, and reflectance is underestimated. This measurement artefact, related to a loss of light at the edges of the illuminated area, is known as the *edge-loss* phenomenon [4].

For colored and opalescent materials, optical properties vary with wavelength, therefore the distance that light can travel within the material, i.e. the size of the material's PSF, varies with wavelength. Consequently, edge-loss varies with wavelength, and affects not only the amplitude of the measured spectral reflectance, but also the spectral distribution. From a colorimetric point of view, edge-loss affects lightness as well as hue. This phenomenon has been observed for applications on restorative materials for dental prosthetics [4–6], where reflectance measurement errors result in very visible aesthetic issues. Edge-loss has also been observed in human skin measurement [7,8], and is referred to as *red-loss* in some skin studies [9]. Indeed, long wavelengths are absorbed less and scattered less than the wavelengths covering the rest of the visible spectrum [10], thus travelling deeper and wider within skin than other wavelengths. When skin reflectance is measured using a spectrophotometer with identical illumination and observation apertures, the edge-loss phenomenon is stronger in the red part of the spectrum, where the measured spectral reflectance is significantly underestimated.

The impact of edge-loss on reflectance measurement is strongly related to the geometry of the measuring device. The highest error is observed for spectrophotometers with identical illumination and observation apertures [4–8], a configuration adapted to strongly scattering materials and found on many devices used in industrial applications. Some instrument suppliers also offer devices featuring different illumination and measurement apertures, which are more adapted to translucent material measurement, such as portable spectrophotometers designed for skin metrology [11]. However, to our knowledge, there are currently no adequate recommendations on how to choose a spectrophotometer depending on the measured material's translucency, a shortcoming that this paper seeks to address.

The International Commission on Illumination (CIE) [12] and the ASTM standard organizations [13] have raised the problem of translucent material measurement and underlined that it requires caution in the choice of measurement configuration. However, no precise recommendations have been given. In a 1976 technical note of the US National Bureau of Standards, Hsia proposes a formal description of edge-loss [14], but the resulting recommendations remain vague: he advises working with large samples, with an illuminated area at least two or three times larger than the observation area. In this article, we propose a study of edge-loss which accounts for both the configuration of the measuring device and the optical properties of the translucent material. Indeed, the requirements on the illuminated and observed areas that minimize edge-loss strongly depend on the measured material: strict requirements apply for highly translucent materials like skin, but a wider range of configurations can be used for less translucent materials like marble. We address the edge-loss issue with a theoretical approach to provide spectrophotometer users information about the most appropriate measuring configurations according to how translucent a material is, restricting our study to infinitively thick objects (or thick enough to prevent light transmission) measured in reflection.

The rest of the paper is organized as follows: fundamental radiometric quantities used in the study are recalled in Section 2; experimental measurements are presented to illustrate the edge-loss phenomenon along with current recommendations in Section 3; the problem is addressed theoretically in Section 4; an example of application on skin is given in Section 5; edge-loss error predictions are presented for several commercial spectrophotometers and several types of material in Section 6; finally, further work and conclusion are presented in Sections 7 and 8.

2. DEFINITIONS

The reflection and scattering properties of an object are characterized by various radiometric quantities formalized by Nicodemus et al. [15], which permits us to describe how much light is reflected (*Reflectance*), in which directions (*Bidirectional Reflectance Distribution Function* – BRDF), and how far light travels within the material before emerging from it (*Bidirectional Scattering-Surface Reflectance Distribution Function* – BSSRDF). When it comes to the study of translucent materials, the concept of *Point Spread Function* (PSF) can be added to these three quantities. We propose in this present section to recapitulate the definitions of Reflectance and PSF, as they will be crucial to the rest of the article.

2.1 Reflectance

Reflectance, a dimensionless quantity, denotes any ratio of reflected flux to incident flux received and emitted by the same surface element. Reflectance generally depends upon wavelength, illumination geometry and orientation (solid angle), observation geometry and orientation (solid angle), polarization and the location of the point of observation [16]. This last parameter is often ignored for uniform materials. Spectral reflectance is defined as the reflectance in successive narrow wavebands of similar bandwidth.

Reflectance is a general concept that has no signification until precise geometries for illumination and observation are specified, since different combinations of illumination and observation geometries generate very different reflectance values. For example, the reflectance of an aluminum mirror illuminated by collimated light at a certain angle is around 0.8 if the observation system captures the specularly reflected light, and 0 otherwise. For a unified approach of these geometries, Nicodemus et al. [15] proposed a classification of nine geometries based on 3 types of solid angles for the incident light and for the captured light (Fig. 1): directional, conical and hemispherical.

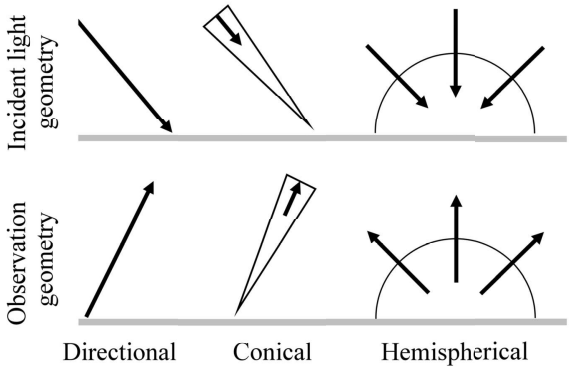

Fig. 1. Possible geometries of illumination and observation for the definition of the reflectance.

Strictly speaking, when the incident light fills a non-infinitesimal cone, its radiance distribution should also be specified. However, when illumination fills conical and hemispherical solid angles, Nicodemus'

classification assumes that the incident radiance is constant. Accordingly, the hemispherical geometry corresponds to a constant radiance over the hemisphere and is also referred to as diffuse. Two of the measurement geometries recommended by the CIE [12] are generally used in commercial spectrophotometers: the (45°a:0°) geometry, which corresponds to an annular illumination at 45° and a directional observation at 0°, and the (d:8°) geometry, which corresponds to a diffuse (or hemispherical) illumination obtained using an integrating sphere, and a directional observation at 8°.

Reflectance is hardly ever measured in practice, because it requires measuring the incident flux, which is very difficult. The measurement of a slightly different quantity called *reflectance factor* is therefore often used instead. Reflectance factor is defined as a ratio of the flux reflected by a surface sample to the flux reflected by a perfect diffuser irradiated in exactly the same way as the sample, collected in the same observation direction.

2.2 Point Spread Function

Light reflection by translucent materials involves light transport aspects that are not described by reflectance. Bidirectional Scattering-Surface Reflectance Distribution Function (BSSRDF) fully describes the spatial and directional aspects of light reflection, but is rather complex to measure or model. To characterize the reflection properties of translucent materials then, Point Spread Function (PSF), describing the spatial aspects of subsurface light scattering, is a simpler alternative which relies on fewer parameters than BSSRDF.

When a translucent material is illuminated punctually, part of the light exits further from the illuminated area due to subsurface scattering, creating a region of diminishing brightness around the point of illumination. The pattern of light observed is the PSF of the material, expressed in m^{-2}. PSF is a function of the incident light geometry, the observation geometry, the position on the surface of the sample, as well as the wavelength and polarization state of light. It is defined as the ratio of the exitance M_o of an infinitesimal area located in $A_o(x_o, y_o)$ to the flux F_i punctually received at the point $A_i(x_i, y_i)$:

$$PSF(x_o, y_o, x_i, y_i) = \frac{M_o(x_o, y_o, x_i, y_i)}{F_i(x_i, y_i)} \quad . \qquad (1)$$

Similarly to reflectance, PSF is characterized by its measurement geometry according to the classification shown in Fig. 1. The incident light flux F_i and the exitance M_o are therefore defined for given illumination and observation solid angles.

PSF can be related to reflectance. When a surface receives a flux F_i punctually in $A_i(x_i, y_i)$, its reflectance can be deduced from the PSF through a spatial integration over an area of observation A centered in A_i, which is sufficiently larger than the spread of the PSF:

$$R(x_i, y_i) = \iint_{(x_o, y_o) \in A} PSF(x_o, y_o, x_i, y_i) dx_o dy_o \quad . \qquad (2)$$

For homogeneous materials, PSF only depends on the distance between A_i and A_o and consequently, reflectance is independent from the incident flux location A_i.

3. MEASURING THE SPECTRAL REFLECTANCE OF TRANSLUCENT MATERIALS USING A SPECTROPHOTOMETER

In practice, spectrophotometers do not provide a reflectance factor measurement on a single point as defined in Section 2.1, but rather the average value over an area of interest. Thus, to fully describe the measurement geometry, the respective sizes of the illuminated and observed areas must be defined in addition to the angular illumination and observation configurations. These additional parameters have a low impact on the measured reflectance for strongly scattering materials, since light subsurface transport is minimal. However, the choice of these parameters is crucial for measuring translucent materials. In this section, we give an experimental illustration of edge-loss impacting translucent material measurement, and present two general measurement configuration recommended by the CIE and ASTM.

3.1 Experimental illustration of the issue

In this study, three industry-oriented spectrophotometers from X-Rite, USA, were used to experimentally illustrate the edge-loss artefact: the Color i7, the Color i1 and the MetaVue™. Three samples were considered (see Fig. 2): the light skin sample of the X-Rite MacBeth® ColorChecker chart, a strongly scattering material; and two translucent materials, skin from the hand palm, and beige soap.

Fig. 2. Color images of the three different samples captured using the MetaVue™ spectrophotometer (X-Rite, USA).

The Color i7 spectrophotometer is a non-portable device that can measure both spectral transmittance and reflectance in the spectral range [360 nm, 750 nm]. The sample receives diffuse light from the whole hemisphere through the use of an integrating sphere. The reflected light is measured at 8° from the normal of the sample. The specular reflection can be included or excluded from the measurement. In this study, the "specular component excluded" (SCE) mode is used. An aperture diameter, defining the illuminated area, can be set to 6 mm, 10 mm, 17 mm or 25 mm. Several configurations are available for defining the lens parameter, which refers to the observed area. By default, the lens parameter is set equal to the aperture diameter, but it can be modified to observe a surface smaller than the aperture. A geometry that minimizes edge-loss is, for example, a 25 mm aperture for illumination, and a 6 mm aperture for observation (this configuration is referred to as "25 - 6 mm" in the spectral reflectances plotted in Fig. 3).

The Color i1 spectrophotometer is a portable device that measures reflectance in the spectral range [360 nm, 750 nm]. The sample is illuminated with an annular source at an angle of 45° with the normal of the sample, and the reflected light is measured in the normal direction. The (45°a:0°) geometry prevents capturing light specularly reflected by smooth or slightly rough surfaces. The illumination and observation areas are disks of respective diameters 4.5 mm and 3.5 mm. Although these areas differ slightly from each other, we will show that this difference is not sufficient to prevent reflectance measurement issues with translucent materials.

The MetaVue™ spectrophotometer is coupled with an imaging system, and measures spectral reflectance in the spectral range [400 nm, 700 nm] in the normal direction, with annular illumination at 45° from the normal over a large area. The manufacturer indicates an aperture diameter of 14 mm, but the illuminated area we observe on the sample is much larger (20 mm by 21 mm). A selection of observation apertures are possible, from 2 to 12 mm.

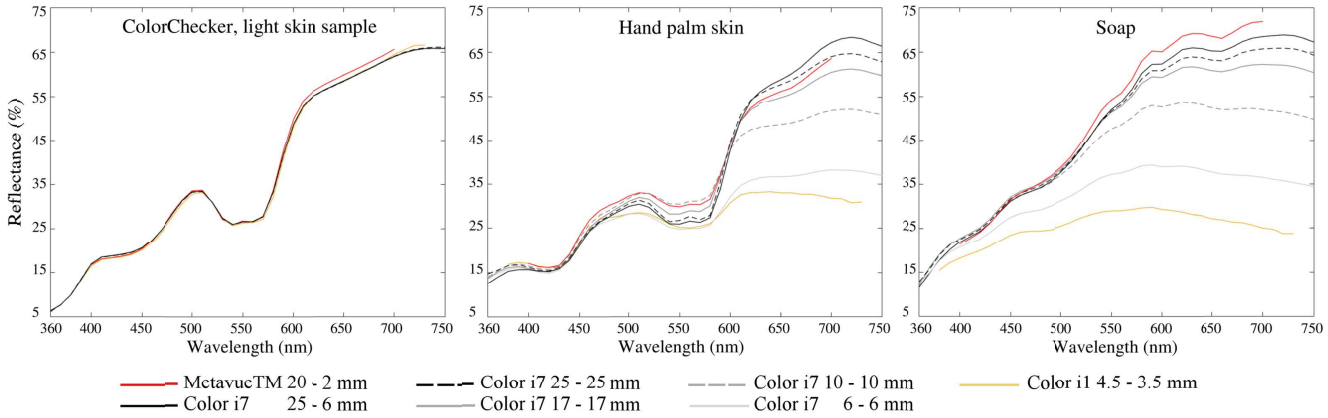

Fig. 3. Spectral reflectance measured using the Color i7, Color i1 and the MetaVue™ spectrophotometers (X-Rite, USA) with varying apertures on three samples: a strongly scattering sample from the ColorChecker (left), hand palm skin (middle) and beige soap (right).

The measured spectral reflectance curves presented in Fig. 3 show that the illumination and observation configurations have no influence on measurements for the strongly scattering material (ColorChecker patch). However, this is not the case for the translucent materials. When using the Color i7 with identical illumination and observation apertures (grey curves and black dotted curve), a smaller aperture causes a higher loss of light, therefore a stronger underestimation of the reflectance. The edge-loss effect is striking in the case of the "6 – 6 mm" and "10 – 10 mm" configurations (identical aperture for illumination and observation of 6 mm and 10 mm, respectively). The spectral reflectances measured with the Color i1 (yellow curves) are the lowest, indicating that this spectrophotometer is particularly not adapted to the measurement of translucent samples.

These results also show that edge-loss is a function of wavelength: for skin and beige soap, edge-loss is larger for large wavelengths (red light). As skin is heterogeneous, spectral variations due to variations in quantities including oxygen rate, blood volume fraction or melanin concentration also affect the different measurements. These variations, however, remain inferior to those that are due to edge-loss in the large wavelengths.

The above measurements suggest that the "25 – 6 mm" configuration of the Color i7 (aperture of 25 mm for illumination and 6 mm for observation, black solid lines on Fig. 3) and the "20 – 2 mm" configuration of the MetaVue™ (red curves on Fig. 3) produce the least erroneous measurements, as they correspond to the reflectance curves with the highest reflectance, particularly in the red wavelengths.

3.2 General recommendations

The CIE and ASTM warn of the particularities of measuring translucent materials, and define several terms to describe these particularities [12,13]. The *sampling aperture* is the aperture delimited by the illuminated area or by the area observed by the sensor, whichever is smaller. If the observed area is larger, and "large enough" to include all the subsurface scattered flux, the observed area is said to be *under filled*. If the illuminated area is larger, and "large enough" compared to the observed area, the observed area is described as *over filled*. These two configurations, illustrated by the dotted arrows in Fig. 4, correspond to the two ways of measuring the spectral reflectance of translucent materials.

In the under filled configuration, all the light that emerges from the material is collected, even when it is outside of the illuminated area, by having an observation area much larger than the illumination area. In the over filled configuration, the small observation area focusses on the center of the illuminated area. Even though part of the incident light illuminating this observed area travels away from the observation scope, the loss is perfectly compensated by the light that has entered into the surrounding area and travelled to the observation scope. According to the Helmholtz reciprocity principle, which states that light traveling from any point P to any point Q in a static scene will follow the same path from Q to P with similar attenuations, the two arrangements yield the same results, except when the sample is photo-luminescent (for which the reciprocity principle does not apply).

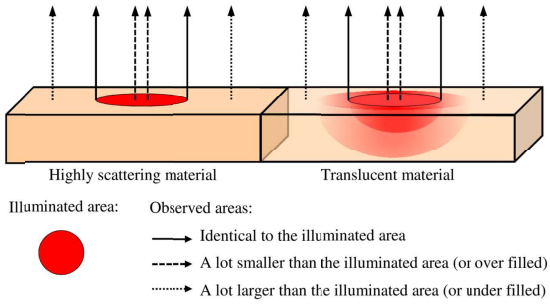

Fig. 4. Possible observation areas for a given illumination on a strongly scattering sample (left) and on a translucent sample (right). The choice of observation area does not affect the measurement for the strongly scattering sample, but it does for the translucent sample.

We notice that most spectrophotometers on the market place that are adapted to measuring translucent material are designed with an observation area smaller than the illuminated area. The opposite configuration appears to be less-often implemented, perhaps because designing a diffuse or annular illumination for an area smaller than the observation area is technically more challenging than the opposite.

Within the definition of these two recommended measurement geometries, the meaning of "large enough" strongly depends on the material optical properties. In the next section, we aim to better characterize the possible measurement geometries by means of a theoretical approach.

4. THEORETICAL ANALYSIS

In this section, a theoretical method is proposed to estimate the error affecting the spectral reflectance measurement of translucent materials due to edge-loss. This error, presented in Section 4.1,

corresponds to the relative difference between the measured reflectance and the actual reflectance of the material, defined in Section 2.1. It depends on the illumination and observation apertures of the measuring device, as well as the PSF of the material. In practice, the PSF of the material is generally not known, but it can be estimated by optical modeling when the material's scattering and absorption coefficients are known. In Section 4.2, we propose to apply the diffusion approximation of the radiative transfer theory [17] to model PSF as a function of the material's optical properties.

4.1 Error estimation method

PSF, defined in Section 2.2, can be used to describe the light pattern, i.e., the spatial exitance function $M_o(x,y)$ that results from a translucent material receiving a spatial irradiance $E_i(x,y)$:

$$M_o(x,y) = (PSF \otimes E_i)(x,y), \quad (3)$$

where $\otimes$ denotes the two-dimensional convolution, defined as:

$$(A \otimes B)(x,y) = \int_u \int_v A(x-u, y-v) B(x,y) du dv. \quad (4)$$

This relationship between PSF, M_o and E_i is illustrated in Fig. 5, in which the considered material is homogeneous and isotropic with a circularly symmetric PSF. In this example, the incident flux also exhibits a symmetry of revolution and can be described by a disk function. The light pattern observed on the illuminated material presents the same properties of symmetry.

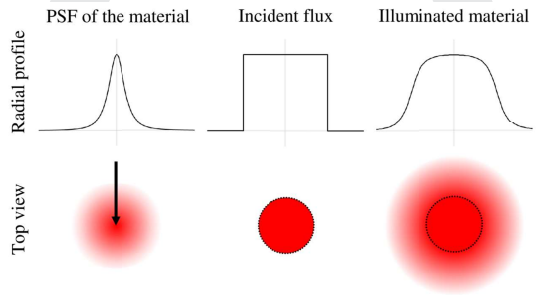

Fig. 5. Schematic representation of the PSF of a translucent material (left), the illumination beam (middle) and the spot of light obtained on the illuminated material (right).

Reflectance, the ratio of reflected to incident fluxes, can be expressed as a function of PSF and incident irradiance $E_i(x,y)$:

$$R = \frac{\iint_A (PSF \otimes E_i)(x,y) dxdy}{\iint_A E_i(x,y) dxdy}, \quad (5)$$

where A represents an area around the illuminated area large enough to collect all the reflected light.

As already mentioned in Section 2.1, reflectance factor $\tilde{R}$ is often measured rather than reflectance, considering a perfect diffuser as reference. Equation (5) yields the following expression for reflectance factor, according to PSF and incident irradiance $E_i(x,y)$:

$$\tilde{R} = \frac{\iint_A (PSF \otimes E_i)(x,y) dxdy}{\iint_A (PSF_{ref} \otimes E_i)(x,y) dxdy}. \quad (6)$$

As light incident on the strongly scattering diffuser is reflected directly off the surface with no subsurface scattering occurring, PSF_{ref} can be described by a Dirac delta function δ:

$$PSF_{ref}(x,y) = \mathrm{k}\,\delta(x,y). \quad (7)$$

The constant k depends on how much light is reflected by the diffuser in the direction of observation. When the reference sample is a perfect diffuser, all the light is reflected uniformly over the full hemisphere, therefore k is 1 for hemispherical observation and $1/\pi$ for directional observation. In practice, spectrophotometers often rely on calibration samples which are not perfect diffusers but for which the value of k has been precisely determined by the manufacturer.

When reflectance factor is measured using a device of finite aperture, the area A corresponds to the observation aperture and the incident irradiance $E_i(x,y)$ depends on the illumination aperture. If A is not large enough to collect all the incident light such that the observation area is under filled, or if A is not small enough to be in the over filled condition defined in Section 3.2, the measured reflectance factor is erroneous. We note ε the relative error between the measured reflectance factor $\tilde{R}_m$ and the actual reflectance factor $\tilde{R}$:

$$\varepsilon = 1 - \tilde{R}_m / \tilde{R}. \quad (8)$$

In order to estimate ε according to the geometry of measurement, let us assume that a translucent sample is illuminated over a disk of diameter d_i and observed over a concentric disk of diameter d_o. Both areas can be described by the disk function D_d expressed in Eq.(9), where d is the diameter of the disk:

$$D_d(x,y) = \begin{cases} 1 & if\ \sqrt{x^2+y^2} < d/2 \\ 0 & otherwise \end{cases}. \quad (9)$$

Using the disk function, the incident irradiance can be written as:

$$E_i(x,y) = \mathrm{E_i}\, D_{d_i}(x,y), \quad (10)$$

where $\mathrm{E_i}$ denotes the irradiance within the disk, assumed to be constant.

The measured reflectance factor $\tilde{R}_m$ can be rewritten from Eq. (6) according to the illumination and observation diameters d_i and d_o, with PSF defined for the same angular configuration as the reflectance measurement:

$$\tilde{R}_m = \frac{\iint_{D_{d_o}} (PSF \otimes \mathrm{E_i}\, D_{d_i})(x,y) dxdy}{\iint_{D_{d_o}} \mathrm{k\,E_i}\, D_{d_i}(x,y) dxdy}. \quad (11)$$

Finally, we note that:

$$\iint_{D_{d_o}} D_{d_i}(x,y) dxdy = \begin{cases} \pi(d_o/2)^2 & if\ d_o \le d_i \\ \pi(d_i/2)^2 & otherwise \end{cases}. \quad (12)$$

Combining Eq. (6), (8), (11) and (12), we obtain:

$$\varepsilon(d_i, d_o) = 1 - \frac{\iint_{D_{d_o}} (PSF \otimes D_{d_i})(x,y) dxdy}{\iint_{D_\infty} (PSF \otimes D_{d_i})(x,y) dxdy} \times \min\left(\frac{{d_i}^2}{{d_o}^2}, 1\right). \quad (13)$$

When the translucent material is homogeneous and isotropic, its PSF has a symmetry of revolution. Thus, Eq. (13) can be written in

polar coordinates [8,14], though convolution in polar coordinates is less straightforward than convolution in Cartesian coordinates [18].

The measurement error ε can be estimated using Eq. (13) as long as the instrument geometry and the PSF of the material are known. The instrument geometry is generally accessible through documentation provided by the manufacturer. However, the PSF is rarely known, especially for a new material. We therefore propose to approximate it, using a generic function based on a small number of parameters, relying on the diffusion approximation model for light subsurface scattering.

4.2 PSF model relying on the diffusion approximation

We propose to model translucent materials as homogeneous media which absorb and scatter light. In the radiative transfer formalism, they are characterized by their optical index n, absorption coefficient μ_a (in m^{-1}), scattering coefficient μ_s (in m^{-1}) and anisotropy parameter g. In practice, the effects of anisotropy are often combined with scattering in the reduced scattering coefficient $\mu_s' = \mu_s (1 - g)$. In order to derive the PSF model, we use the diffusion equation, an approximation of the radiative transfer theory valid for poorly absorbing materials ($\mu_a << \mu_s'$), at distances to the source higher than the scattering mean free path ($\sim 1/\mu_s'$) and under the assumption that, for sufficiently dense materials, the light distribution becomes nearly isotropic after several scattering events, even if single scattering in the material is anisotropic ($g \neq 0$) [17]. The diffusion approximation has been preferred to much more precise models, such as Monte Carlo simulations, for its trade-off between accuracy and computation speed.

Let us consider a semi-infinite and homogeneous material of absorption coefficient μ_a, scattering coefficient μ_s' and optical index n, illuminated by a light beam. Under the assumptions of the diffusion approximation, the diffuse irradiance (also called fluence rate in the literature [17], in $W.m^{-2}$) $\phi(x, y, z)$ at any depth z in the material satisfies the following equation:

$$-D\Delta\phi + \mu_a \phi = S_d \quad , \tag{14}$$

where $D = 1/(3\mu_t)$ is the diffusion coefficient with $\mu_t = \mu_a + \mu_s'$, Δ is the Laplace operator, and S_d is the diffuse source irradiance distribution.

In order to model the PSF of the material under any illumination, e.g., directional, annular or diffuse, we first consider that the material is illuminated by an infinitesimally thin collimated light beam oriented according to the direction (θ, φ), where θ denotes the polar angle in respect to the normal of the surface, and φ the azimuth angle.

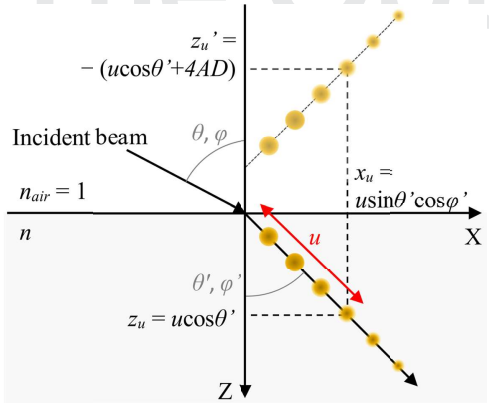

Fig. 6. An oblique incident light beam is converted into a line of dipole sources for the resolution of the diffusion equation according to the line source method.

When the incident light is normal to the surface, it is easier to solve the diffusion equation using the dipole method introduced by Patterson et al. [19,20], in which the incident light is converted into a single punctual isotropic source located inside the material, paired together with a virtual source located outside the material, such that the boundary conditions are satisfied. In the case of oblique illumination, however, the dipole approximation is poorly adapted as it does not model correctly the asymmetry of the PSF [21]. To properly deal with oblique illumination, the incident light can be converted into a collection of point sources distributed along the incident refracted beam inside the material, with exponentially decreasing intensities. Again, the boundary conditions are satisfied by pairing each source with a virtual source outside the material. This *line source* method is illustrated in Fig. 6.

We refer to the works of Farrell et al [20] and Donner and Jensen [22] for the implementation of this line source method. Let us consider a point source located inside the material, at a distance u from the surface along the incident refracted beam. The Cartesian coordinates of this point source are:

$$(x_u, y_u, z_u) = (u\sin\theta'\cos\varphi',\ u\sin\theta'\sin\varphi',\ u\cos\theta') \quad , \tag{15}$$

with (θ', φ') characterizing the refracted beam direction: $\theta' = \sin^{-1}(\sin(\theta)/n))$ and $\varphi' = \varphi + \pi$.

The boundary conditions are taken into account by adding a virtual source outside the material, at a position:

$$(x_u', y_u', z_u') = (x_u,\ y_u, -(z_u + 4AD)) \quad , \tag{16}$$

with

$$A = (1 + R_{eff}) / (1 - R_{eff}) \quad , \tag{17}$$

where R_{eff} is the effective reflection coefficient which accounts for the light reflection at the air-material interface. It depends on the optical index n of the material: $R_{eff} \approx 0.0636n + 0.6681 + 0.7099/n - 1.4399/n^2$ [23].

This point source, whose flux is considered unitary, creates with its corresponding virtual source the diffuse exitance M_u at a point (x,y) of the surface, given by:

$$M_u(x,y) = \frac{1}{4\pi}\left[z_u\left(\mu_{eff} + \frac{1}{d_u}\right)\frac{e^{-\mu_{eff} d_u}}{{d_u}^2} + z_u'\left(\mu_{eff} + \frac{1}{d_u'}\right)\frac{e^{-\mu_{eff} d_u'}}{{d_u'}^2} \right] \quad , \tag{18}$$

where

$$\mu_{eff} = \sqrt{3\mu_a\mu_t}$$
$$d_u = \sqrt{(x - x_u)^2 + (y - y_u)^2 + {z_u}^2}$$
$$d_u' = \sqrt{(x - x_u)^2 + (y - y_u)^2 + (z_u + 4AD)^2} \quad . \tag{19}$$

The total exitance $M_{\theta,\varphi}(x,y)$ at the surface is obtained by considering an infinite number of sources along the refracted light beam and summing the exitance given by Eq. (18) for each source of flux $F(u)$:

$$M_{\theta,\varphi}(x,y) = \int_0^\infty F(u) M_u(x,y) du \quad . \tag{20}$$

The flux $F(u)$ of each source decreases exponentially with the source location u along the refracted beam. However, since most materials are

anisotropic, the light near the point of incidence is not sufficiently scattered to reach the isotropic scattering regime. To account for this, a phase function correction can be applied when the scattering phase function is known [21]. We have followed the suggestion of Donner and Jensen [22] to add, as an approximation, an attenuation coefficient $K(u) = 2(1-\exp(-\mu_t u))$ to the source power. Therefore, for an incident beam of flux F_0, a spatial distribution along the refracted beam du, and a material of reduced albedo $a' = \mu_s'/\mu_t$, the source flux $F(u)$ can be written as:

$$F(u) = 2F_0 a' \mu_t e^{-\mu_t u}(1-e^{-\mu_t u})du \quad . \tag{21}$$

It verifies:

$$\int_0^\infty F(u)du = a'F_0 \quad . \tag{22}$$

The total exitance is:

$$M_{\theta,\varphi}(x,y) = \frac{2\mu_s' F_0}{4\pi}\int_0^\infty e^{-\mu_t u}(1-e^{-\mu_t u}) \left[z_u \left(\mu_{eff} + \frac{1}{d_u}\right)\frac{e^{-\mu_{eff} d_u}}{{d_u}^2} + z_u' \left(\mu_{eff} + \frac{1}{d_u'}\right)\frac{e^{-\mu_{eff} d_u'}}{{d_u'}^2} \right] du \quad . \tag{23}$$

Finally, the PSF of the material for an oblique illumination of direction (θ, φ) and a diffuse observation is obtained by dividing the exitance by the flux punctually received at the surface:

$$PSF_{(\theta,\varphi:\mathrm{d})}(x,y) = \frac{M_{\theta,\varphi}(x,y)}{F_0} \quad . \tag{24}$$

From Eqs. (23) and (24), we can now compute the material's PSF for any illumination configuration and diffuse observation.

Figure 7 shows PSF profiles calculated using the line source method for normal and oblique illuminations for a material with μ_a = 0.01 mm^{-1}, μ_s' = 1 mm^{-1} and n = 1.4. It illustrates the asymmetric PSF obtained for oblique illuminations.

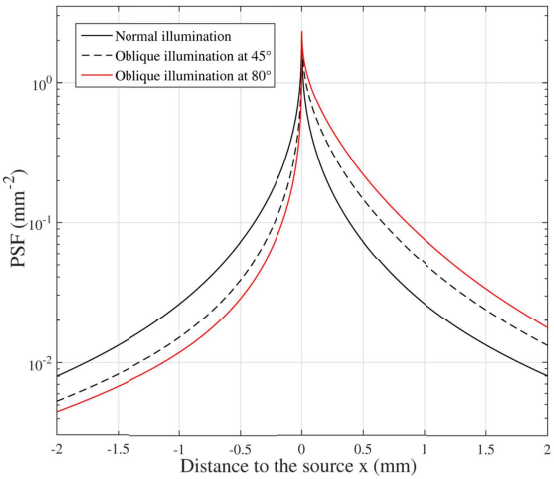

Fig. 7. PSF profiles for normal and oblique illuminations using the line source method for μ_a = 0.01 mm^{-1}, μ_s' = 1 mm^{-1} and n = 1.4.

For normal, annular at 45° and diffuse illuminations, we obtain symmetric PSF whose expressions are:

$$PSF_{(0°:\mathrm{d})}(x,y) = M_{0°,0°}(x,y)/F_0$$

$$PSF_{(45°\mathrm{a}:\mathrm{d})}(x,y) = \frac{1}{2\pi F_0}\int_{\varphi=0}^{2\pi} M_{45°,\varphi}(x,y)d\varphi$$

$$PSF_{(\mathrm{d}:\mathrm{d})}(x,y) = \frac{1}{2\pi F_0}\int_{\theta=0}^{\pi/2}\int_{\varphi=0}^{2\pi} M_{\theta,\varphi}(x,y)\sin\theta d\varphi d\theta \quad . \tag{25}$$

Figure 8 shows the PSF profiles for these configurations and the same material (μ_a = 0.01 mm^{-1}, μ_s' = 1 mm^{-1} and n = 1.4). We can note that even for a normal illumination, the curve obtained using the line source method (plotted in solid black), cannot be substituted by the curve obtained using the dipole approximation (plotted in yellow) when accuracy is required at the center of the PSF.

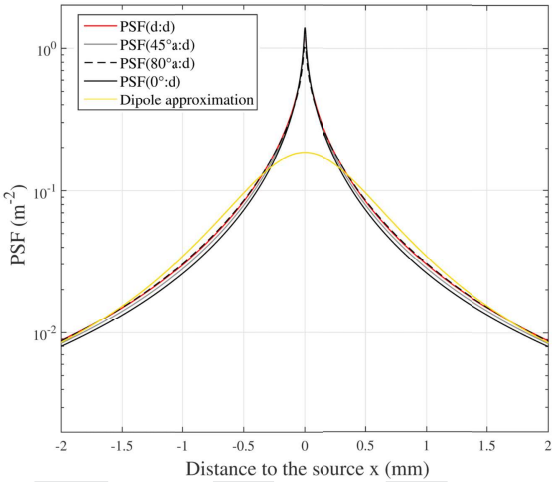

Fig. 8. PSF Profile for various illumination conditions estimated using the line source method and the dipole approximation (normal illumination) for μ_a = 0.01 mm^{-1}, μ_s' = 1 mm^{-1} and n = 1.4.

Regarding the curves corresponding to oblique annular illuminations (see PSF(45°a:d) in grey and PSF(80°a:d) in dotted black, respectively corresponding to an annular illumination at 45° and 80°), as expected, annular illumination reestablishes the circular symmetry of the PSF although oblique illumination creates asymmetric PSFs as shown in Fig. 7. However, we did not anticipate that there would be such a small difference between the PSF curves corresponding to a normal collimated beam (see PSF(0°:d) in solid black) and an annular illumination at a low angle (see PSF(45°a:d)). When the incident angle θ of the annular illumination increases (see PSF(80°a:d)), the PSF profile remains very close to PSF(0°:d) at the center, and is slightly higher further from the center. Similar observations can be made from Fig. 8 with PSF(d:d) (diffuse illumination, in red), which is slightly higher than PSF(0°:d) further from the center.

Regarding the geometry of observation, when the diffusion approximation applies, the diffuse light that exits the material can be assumed as Lambertian, i.e., reemitted with the same radiance in any direction of the hemisphere. In such cases, capturing light in any direction θ within this cone corresponds to capturing a fraction of the light reflected in the full hemisphere:

$$PSF_{(\mathrm{i}:\theta°)} = \frac{1}{\pi} PSF_{(\mathrm{i}:\mathrm{d})} \quad . \tag{26}$$

The relative measurement error expressed by Eq. (13) is invariant to PSF multiplication by a constant. Consequently, using this theoretical

model, the predicted error remains the same for a diffuse observation or a directional observation.

In the following sections, given that there is little observable difference between the curves of Fig. 8, the PSF for a normal collimated beam will be used rather than the PSF for an annular or diffuse illumination, as it allows for shorter calculation time. In addition, given that the edge-loss error is invariant to multiplication by a constant as mentioned above, the model of PSF that will be used is that which is valid in the (0°:d) configuration although the usual geometries of measurement are (d:8°) and (45°a:0°).

5. APPLICATIONS ON HUMAN SKIN

Skin is a translucent material of considerable interest for applications in various fields including medicine, dermatology, cosmetology and computer graphics. To study the impact of edge-loss on skin measurement, we use in this section the PSF model presented in Section 4.2 [Eq.(23)] by considering parameter values at the wavelength 700 nm issued from the literature for light-colored skin: μ_a = 0.05 mm^{-1} for the absorption coefficient [10], μ_s' = 1.5 mm^{-1} for the reduced scattering coefficient [24] and n = 1.4 for the optical index [10]. The selected wavelength corresponds to that in the visible spectral domain for which skin is the least absorbent and the least scattering, and therefore, for which measurement error due to edge-loss is highest.

We consider illumination and observation apertures, each varying between 1 and 50 mm. The PSF of the material is modeled for a normal directional illumination, the configuration that is the fastest to compute in Matlab (MathWorks, US), under the assumption that is it close to the PSF for diffuse or annular illumination with a directional observation, as discussed in Section 4.2.

Figure 9 displays the relative error for the reflectance measurement predicted according to Eq. (23) for any observation and illumination aperture couple within the considered range. On these 2D graphs, the abscissa corresponds to the size of the observation aperture, and the ordinate the size of the illumination aperture.

The graphs confirm that error is higher when the observation and illumination apertures are the same size. In such a configuration, according to our theoretical prediction, an aperture larger than 20 mm is required to achieve an error below 10%, and an aperture larger than 40 mm is required to achieve an error below 5%.

When the observation and illumination apertures differ from one another, the relative error decreases significantly. The same error is observed when the illumination and observation aperture sizes are reversed. This is consistent with the Helmholtz reciprocity principle for light paths. We can therefore refer to either the illuminated or observed area, whichever is larger, as the *measurement area*.

The smaller the measurement area, the larger the difference needed between observation and illumination apertures to obtain low measurement error. For example, for a 20 mm diameter measurement area, the difference needed to obtain less than 5% measurement error is 2 mm. Conversely, for a 12 mm measurement area, the difference needed to obtain less than 5% measurement error is 5 mm. According to our simulations, the measurement area on skin must be larger than 7 mm to obtain less than 10% error at 700 nm.

These theoretical predictions can be compared with the experimental measurements presented in Section 3.1. Experimentally, the true value for skin reflectance factor $\tilde{R}$ cannot be measured with the spectrophotometers at our disposal, as none of them offer illumination apertures sufficiently large and observation apertures sufficiently small to guarantee no measurement error on skin at 700 nm. Therefore, it is not possible to compute the relative measurement error from the measured reflectance factor $\tilde{R}_m$. However, it is possible to compute the deviation γ defined as the relative difference between $\tilde{R}_m$, the reflectance measured for a set of illumination and observation apertures (d_i, d_o), and $\tilde{R}_{m,ref}$, the reflectance measured in the configuration ($d_{i,ref}$, $d_{o,ref}$):

$$\gamma(d_i, d_o, d_{i,ref}, d_{o,ref}) = 1 - \frac{\tilde{R}_m}{\tilde{R}_{m,ref}} . \quad \textbf{(27)}$$

From the definition of the relative measurement error ε given in Section 4.1 [Eq.(8)], we also note that, for any configuration x:

$$\tilde{R}_{m,x} = (1 - \varepsilon(d_{i,x}, d_{o,x}))\tilde{R} . \quad \textbf{(28)}$$

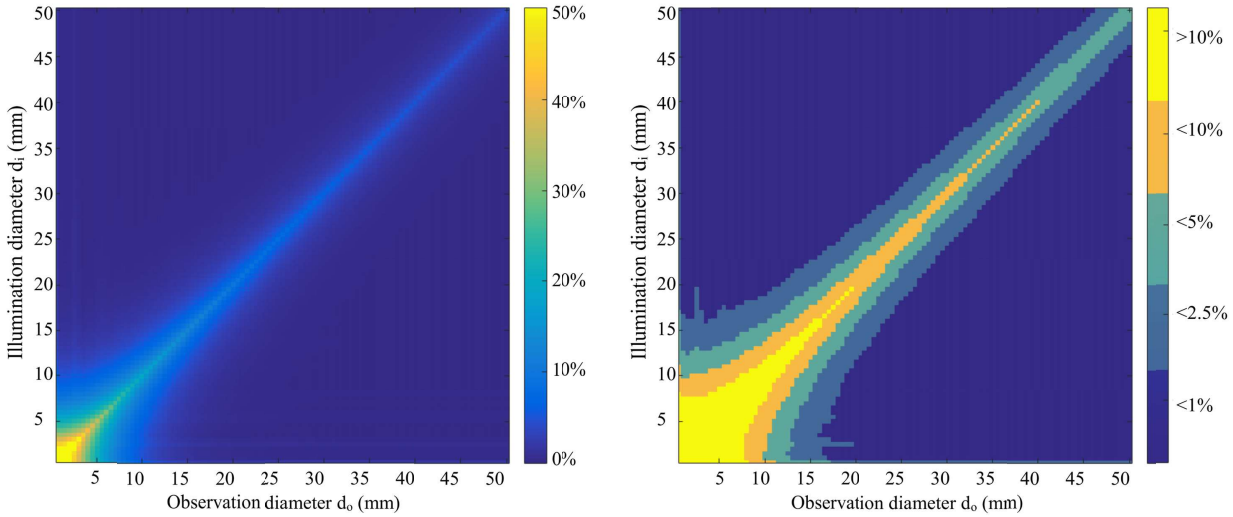

Fig. 9. Predicted relative error (%) for skin reflectance measurement at 700 nm (μ_a = 0.05 mm^{-1}, μ_s' = 1.5 mm^{-1} and n = 1.4) for various illumination and observation apertures. The same graph is plotted with two different color scales, a continuous one and a discreet one. The discreet scale is for an easier reading of the percentage of error.

Therefore, the deviation γ can be expressed according to the errors $\varepsilon(d_i, d_o)$ and $\varepsilon(d_{i,ref}, d_{o,ref})$ calculated using Eq. (13):

$$\gamma(d_i, d_o, d_{i,ref}, d_{o,ref}) = 1 - \frac{1-\varepsilon(d_i, d_o)}{1-\varepsilon(d_{i,ref}, d_{o,ref})} \quad \textbf{(29)}$$

For skin at 700 nm, Eq. (27) is used to estimate the experimental deviation for several measurement configurations of the Color i7 (SCE, (d:8°)), relatively to the configuration "25 mm – 6 mm" corresponding to a 25 mm illumination aperture and a 6 mm observation aperture. Equation (29) is used to compute the theoretical values for this deviation. Both experimental and theoretical deviations are presented in Table 1.

Table 1. Experimental and theoretical deviations $\gamma(d_i, d_o, 25\text{ mm}, 6\text{ mm})$ for skin reflectance measurement at 700 nm. The reference measurement considered here corresponds to a 25 mm illumination aperture and a 6 mm observation aperture ($d_{i,ref}$ = 25 mm, $d_{o,ref}$ = 6 mm).

d_i	d_o	Experimental deviation γ	Theoretical deviation γ
6 mm	6 mm	44%	31%
10 mm	10 mm	24%	20%
17 mm	17 mm	11%	12%
25 mm	25 mm	5.6%	8.0%

Table 1 shows that the experimental deviations are mostly consistent with the deviations predicted by the model, especially for apertures 10 and 17 mm. However, the model tends to underestimate the measurement error for a small aperture (6 mm), and overestimate it for a large aperture (25 mm). Several reasons for this have been identified.

Firstly, the optical coefficients used in the prediction might not correspond to the actual properties of the measured area of skin. In particular, the selected μ_a value (μ_a = 0.05 mm^{-1}) is rather arbitrary: literature provides average values, but skin absorption properties are highly heterogeneous, strongly varying from one person to another or in different locations on the body.

Secondly, modeling skin as a uniform single layer material is perhaps an overly simplistic approximation [25]. It is very likely that considering two layers or more would yield a more accurate model of skin PSF [26].

Lastly, the PSF model itself has limitations: the diffusion approximation is not valid close to the point source, that is at the center of the PSF, where it underestimates the amount of reflected light [27]. This suggests that the model tends to overestimate the portion of light reflected far from the source, which might induce an overestimation of the measurement error. It is not clear to what extent this issue, which is not specific to skin, affect the predictions. For measuring skin, a more accurate PSF model could improve the prediction accuracy, for example by using a very detailed model of skin and a Monte Carlo method to predict light propagation in skin. For objects that can be described as homogeneous and semi-infinite, further studies are required to identify whether or not a more accurate PSF model significantly improves the prediction accuracy.

6. COMMERCIAL SPECTROPHOTOMETERS PERFORMANCES FOR VARIOUS DEGREES OF TRANSLUCENCY

For skin and biological tissues, the predictions presented in the previous section are possible thanks to many optical coefficients published in the biomedical optics literature. However, for many other translucent materials, optical coefficients are not precisely known.

We propose to classify materials into three broad categories of translucency, limiting our study to materials with $\mu_s' \geq 1$ mm^{-1} for which the diffusion approximation is valid [17]. As already explained in the introduction, we are interested here in optical translucency rather than perceptual translucency, for which translucency scales also exist. This optical translucency is considered to be low when the material's PSF is narrow, due to a rather high scattering coefficient, to be high when the PSF is large, due to a rather low scattering coefficient, and to be medium for an intermediate PSF size.

In this section, the theoretical approach detailed in Section 4 is used to predict for each degree of translucency the magnitude of edge-loss error obtained when using various commercial spectrophotometers.

Let us consider materials with the following reduced scattering coefficients to describe the three degrees of translucency: μ_s' = 5 mm^{-1} for low translucency, μ_s' = 2 mm^{-1} for medium translucency and μ_s' = 1 mm^{-1} for high translucency. The absorption coefficient we choose at first is rather low (μ_a = 0.01 mm^{-1}), in order to model materials for which edge-loss is an important issue. A higher absorbance would reduce subsurface light transport and produce narrower PSFs, which correspond to lower translucency for the same reduced scattering coefficient values. Figure 10 represents the normalized PSF of these three virtual materials, predicted by the model (Eq. (23) with (θ, φ)=(0°, 0°) and n = 1.4).

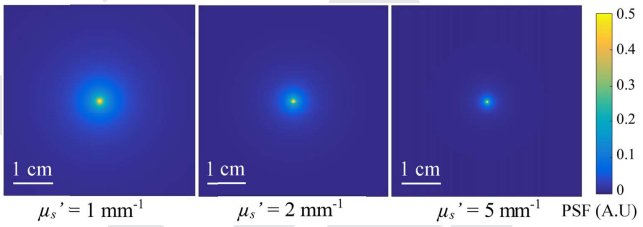

Fig. 10. Predicted PSF normalized such that its value at the center is 1 and displayed in false colors, for materials of various μ_s' and fixed μ_a = 0.01 mm^{-1}.

To better understand these different degrees of translucency, various examples of common materials that fall within the specified ranges are given in Table 2 [24,28]. We would like to note that by covering the material with a layer of strongly scattering medium, such as powder or white paint, translucency is strongly decreased. By doing so, the reflectance measurement becomes less sensitive to the illumination and observation areas. This is for the case with human skin when it is covered by make-up or foundation.

Table 2. Example of translucent materials [24,28].

μ_s' (mm^{-1})	Translucency	Example of materials
≈ 1	High	Skin (near infrared), apple flesh, beeswax
≈ 2	Medium	Milk, skin (red and green wavelengths), cocoa butter
≈ 5	Low	Marble, cream, skin (blue wavelengths)

Several spectrophotometer manufacturers offer measuring devices with illumination apertures larger than the observation aperture, thus allowing reflectance measurements on translucent materials. The considered spectrophotometers, from X-Rite (US), Barbieri Electronic

(Italy), Konika Minolta (Japan) and BYK-Gardner (Germany), are characterized by their illumination and observation apertures d_i and d_o given by the manufacturer. Using the theoretical method developed in Section 4, the predicted measurement errors for these spectrophotometers have been calculated for each degree of translucency. The predicted errors, given in Table 3, are plausible, but approximate, given the fact that the diffusion approximation model that we used has limited accuracy in some cases, as discussed above.

Table 3. Estimated measurement error of several commercial spectrophotometers for various degrees of translucency (with μ_s' in mm^{-1} and μ_a = 0.01 mm^{-1}).

μ_a = 0.01 mm^{-1} Measurement device	Apertures		Estimated error		
	d_i	d_o	High translucency μ_s' = 1 mm^{-1}	Medium translucency μ_s' = 2 mm^{-1}	Low translucency μ_s' = 5 mm^{-1}
X-Rite Color i7	25 mm	6 mm	5%	1%	0.3%
	10 mm	6 mm	29%	15%	4%
X-Rite MetaVue™	20 mm	2 mm	8%	2.2%	0.4%
Barbieri Spectro LFP	8 mm	2 mm	33%	17%	5%
Konika Minolta CM-700d	11 mm	8 mm	28%	15%	4%
BYK-Gardner Spectro2guide	12 mm	8 mm	24%	12%	3%

The estimated error values presented in Table 3 show that the type of measuring device strongly impacts the amount of edge-loss. The lowest error values are obtained when the illuminated area is large, and when it is significantly larger than the observed area.

The most highly translucent materials (μ_s' = 1 mm^{-1}) are the most problematic to accurately measure: an error below 5% cannot be obtained using any of the tested devices. However, all of the considered devices perform well on materials with low translucency (μ_s' = 5 mm^{-1}): error does not exceed 5% for any of them.

For samples with medium translucency (μ_s' = 2 mm^{-1}), such as human skin between 500 and 700 nm, the choice of device significantly affects the reflectance measurement accuracy. Reflectance measurements are least affected by edge-loss using the "25 – 6 mm" option of the X-rite Color i7 spectrophotometer, where the illumination aperture is 25 mm and the observation aperture is 6 mm, or the "20 – 2 mm" option of the X-rite MetaVue™ spectrophotometer, corresponding to a 20 mm illumination aperture and a 2 mm observation aperture. For these two configurations, it is necessary to have samples that are sufficiently large and sufficiently homogeneous, which is not always possible. When the sample is smaller (12 mm or less in diameter), the four configurations offered by the four spectrophotometers suppliers considered here are equivalent.

With more absorbent materials, the estimated errors are strongly reduced. Choosing a slightly higher absorption coefficient of μ_a = 0.05 mm^{-1} rather than 0.01 mm^{-1}, the error remains below 1% for materials with low translucency (μ_s' = 5 mm^{-1}) and below 6% for materials of medium translucency (μ_s' = 2 mm^{-1}). For materials for which μ_s' = 1 mm^{-1}, however, absorption needs to be higher for all spectrophotometers for accurate measurements.

7. FURTHER WORK

We have limited our study to the measurement of infinitely thick objects through which light cannot pass, however, the measurement of spectral reflectance and transmittance of thin translucent materials raises similar questions, with additional parameters such as interface effects, sample thickness or 3D shape. As it is not always possible to ensure very thick planar samples, a wider study including these configurations would be useful.

To take this study further, edge-loss phenomenon could also be used to estimate the optical properties of translucent materials, which would be of great use to the study of skin in vivo. There currently exist several methods relying on reflectance measurement and optical modeling for estimating the scattering and absorption properties of a material, however, they are not adapted for skin in vivo measurement, as they rely on measuring the material in two different configurations, such as in reflection and transmission, on black and white backings [29], or for two different thicknesses of the material [30]. These configurations are not adapted to thick materials that cannot be altered, like skin, or art glaze in the domain of cultural heritage. Measuring reflectance using different configurations that are differently impacted by edge-loss, along with an optical model describing the phenomenon, could present a solution to estimating the absorption and scattering properties of a material. Such a method has been implemented for skin characterization by Yoshida et al. [31], who uses the dipole approximation to model PSF. A similar method has been proposed in the field of 3D printing by Urban et al. [32], who use reflectance measurements impacted by edge-loss to define a translucency index. These approaches seem promising for the development of potentially compact and low-cost optical devices, especially for applications to skin study.

8. CONCLUSION

In this study, we have proposed a theoretical approach to edge-loss, with the PSF of translucent materials modeled using the diffusion approximation of the radiative transfer theory. The model was applied to predict edge-loss measurement error according to the sizes of the illumination and observation areas, and the material's optical properties. The theoretical results obtained here show that the correct choice of illumination and observation areas strongly depends on the optical translucency of the material. Commercial devices for translucent material measurement are mostly adequate for measuring materials with low translucency, but the spectrophotometers referenced here all demonstrated significant shortcomings when it came to highly translucent materials. For samples of intermediate translucency, the accuracy of the measurement varied depending on the measurement configuration, with large measured areas yielding

better results. For large samples, accurate reflectance measurement can be obtained with several devices. However, when the measured sample is too small or not homogeneous on a sufficiently large area, materials of medium and high translucency remain difficult to measure. For example, measuring the spectral reflectance of the human lip using a commercial spectrophotometer seems particularly challenging. In such cases, hyperspectral imaging [26] can be a good alternative, as the illuminated area can be very large, and the observation area, corresponding to the area imaged by a single pixel of the camera, can be very small.

Disclosure. The authors declare no conflicts of interest.

Funding. This work was supported by the Région Auvergne-Rhône-Alpes (ARC 6), the French National Research Agency (ANR) within the LABEX MANUTECH-SISE (ANR-10-LABX-0075) program of Université de Lyon, and the EMPIR program co-financed by the Participating States and from the European Union's Horizon 2020 research and innovation program.

References

1. J. Dupuy and J. Wenzel, "An adaptive parameterization for efficient material acquisition and rendering." ACM Trans. Graph **37**, 6, 1-14 (2018).
2. M. Gerardin, L. Simonot, J.-P. Farrugia, T. Fournel, and M. Hébert, "A translucency classification for computer graphics," in *Electronic Imaging*, Vol. 6, 203–1 (2019).
3. D. Gigilashvili, P. Urban, J. B. Thomas, J. Y. Hardeberg, and M. Pedersen, "Impact of Shape on Apparent Translucency Differences." in *Color and Imaging Conference*, vol. 2019, no. 1, pp. 132-137 (2019).
4. R. A. Bolt, J. J. Ten Bosch, and J. C. Coops, "Influence of window size in small-window colour measurement, particularly of teeth," Phys. Med. Biol. **39**, 1133–1142 (1994).
5. Y.-K. Lee, B.-S. Lim, and C.-W. Kim, "Influence of illuminating and viewing aperture size on the color of dental resin composites," Dental Materials **20**, 116–123 (2004).
6. W. M. Johnston, N. S. Hesse, B. K. Davis, and R. R. Seghi, "Analysis of Edge-losses in Reflectance Measurements of Pigmented Maxillofacial Elastomer," J. Dent. Res. **75**, 752–760 (1996).
7. H. Takiwaki, Y. Miyaoka, N. Skrebova, H. Kohno, and S. Arase, "Skin reflectance-spectra and colour-value dependency on measuring-head aperture area in ordinary reflectance spectrophotometry and tristimulus colourimetry," Skin Res Technol **8**, 94–97 (2002).
8. K. Yoshida, N. Komeda, N. Ojima, and K. Iwata, "Simple and effective method for measuring translucency using edge loss: optimization of measurement conditions and applications for skin," J. Biomed. Opt. **16**, 117003 (2011).
9. L. Vidovič, M. Milanič, L. L. Randeberg, and B. Majaron, "Quantitative characterization of traumatic bruises by combined pulsed photothermal radiometry and diffuse reflectance spectroscopy," in *Photonic Therapeutics and Diagnostics XI* (SPIE, 2015), Vol. 9303, 930307.
10. S. L. Jacques, "Optical properties of biological tissues: a review," Phys. Med. Biol. **58**, R37–R61 (2013).
11. X-Rite, "CAPSURE(TM) Cosmetic," https://www.xrite.com/categories /portable- spectrophotometers/capsure-cosmetic. (Accessed on 6 June 2020).
12. CIE, Colorimetry, 3rd Edn. (Bureau Central de la CIE, 2004).
13. ASTM International, *Standard Practice for Specifying the Geometries of Observation and Measurement to Characterize the Appearance of Materials* (2011).
14. J. J. Hsia, *The Translucent Blurring Effect: Method of Evaluation and Estimation*. (National Bureau of Standards, 1976).
15. F. E. Nicodemus, J. C. Richmond, J. J. Hsia, I. W. Ginsberg, and T. Limperis, *Geometrical Considerations and Nomenclature for Reflectance* (National Bureau of Standards, 1977).
16. R. McCluney, *Introduction to Radiometry and Photometry*, Artech House (1994).
17. A. Ishimaru, *Wave Propagation and Scattering in Random Media, Single Scattering and Transport Theory*, Vol. 1, Academic Press (1978).
18. N. Baddour, "Two-Dimensional Fourier Transforms in Polar Coordinates," in *Advances in Imaging and Electron Physics*, Vol. 165, 1–45 (2011).
19. M. S. Patterson, E. Schwartz, and B. C. Wilson, "Quantitative Reflectance Spectrophotometry For The Noninvasive Measurement Of Photosensitizer Concentration In Tissue During Photodynamic Therapy," in *Proc. SPIE 1065, Photodynamic Therapy: Mechanisms* (1989).
20. T. J. Farrell, M. S. Patterson, and B. Wilson, "A diffusion theory model of spatially resolved, steady-state diffuse reflectance for the noninvasive determination of tissue optical properties in vivo," Med Phys **19**, 879–888 (1992).
21. R. J. Zemp, "Phase-function corrected diffusion model for diffuse reflectance of a pencil beam obliquely incident on a semi-infinite turbid medium," J. Biomed. Opt. **18**, 067005 (2013).
22. C. Donner and H. W. Jensen, "Rendering translucent materials using photon diffusion," in *ACM SIGGRAPH 2008 Classes on - SIGGRAPH '08* (2008).
23. M. Keijzer, W. M. Star, and P. R. M. Storchi, "Optical diffusion in layered media," Appl. Opt **27**, 1820 (1988).
24. H. Jonasson, et al., "In vivo characterization of light scattering properties of human skin in the 475- to 850-nm wavelength range in a Swedish cohort," J. Biomed. Opt. **23**, 1 (2018).
25. T. Igarashi, K. Nishino, and S. K. Nayar, "The Appearance of Human Skin: A Survey," Foundations and Trends in Computer Graphics and Vision **3**, 1–95 (2007).
26. L. Gevaux, C. Adnet, P. Séroul, R. Clerc, A. Trémeau, J. L. Perrot, and M. Hébert, "Three-dimensional maps of human skin properties on full face with shadows using 3-D hyperspectral imaging," J. Biomed. Opt. **24**, 1 (2019).
27. F. Foschum, M. Jäger, and A. Kienle, "Fully automated spatially resolved reflectance spectrometer for the determination of the absorption and scattering in turbid media," Rev. Sci. Instrum. **82**, 103104 (2011).
28. H. W. Jensen, S. R. Marschner, M. Levoy, and P. Hanrahan, "A practical model for subsurface light transport," in *Proceedings of the 28th Annual Conference on Computer Graphics and Interactive Techniques - SIGGRAPH '01* (2001).
29. R. Levinson, P. Berdahl, and H. Akbari, "Solar spectral optical properties of pigments — Part I: model for deriving scattering and absorption coefficients from transmittance and reflectance measurements," Solar energy materials and solar cells *89*, 319–349 (2005).
30. M. Doi, R. Ohtsuki, and S. Tominaga, "Spectral estimation of made-up skin color under various conditions," in *Proc. SPIE 5008, Color Imaging VIII: Processing, Hardcopy, and Applications* (2003).
31. K. Yoshida, "Derivation of absorption coefficient and reduced scattering coefficient with edge-loss method and comparison with video reflectometry method," Optical Review **23**, 579–586 (2016).
32. P. Urban, T. M. Tanksale, A. Brunton, B. M. Vu, and S. Nakauchi, "Redefining A in RGBA: Towards a Standard for Graphical 3D Printing," ACM Trans. Graph. **38** (2019).